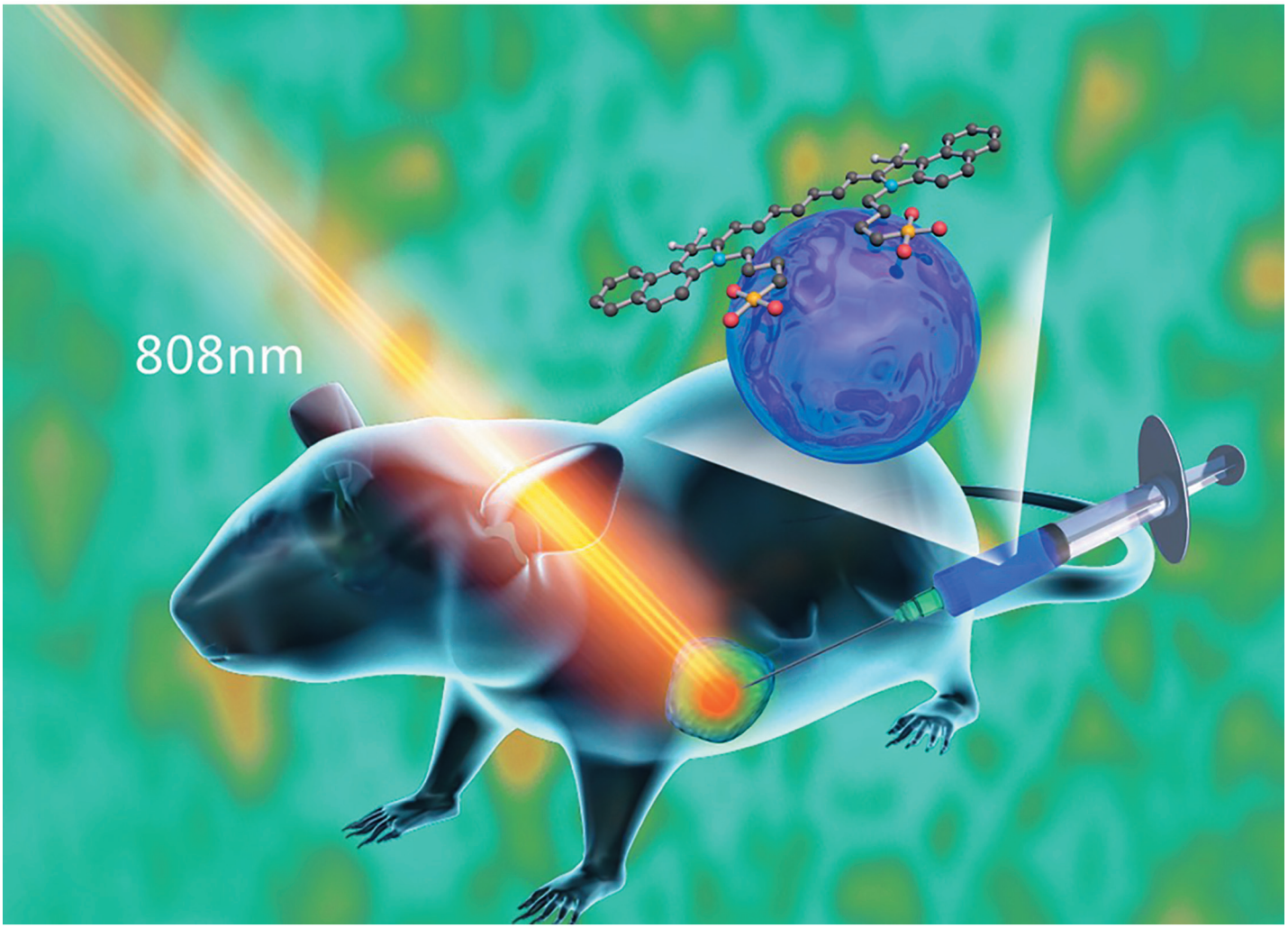

Showcasing joint research from Professor Lovell's laboratory, Department of Biomedical Engineering, State University of New York at Buffalo, USA; and Dr. Jin's laboratory at Union Hospital, Tongji Medical College and Huazhong University, Wuhan, China.

Indocyanine green binds to DOTAP liposomes for enhanced optical properties and tumor photoablation

Enhancing theranostic capabilities of a commonly-used near infrared dye: Indocyanine green is shown to have enhanced properties for imaging and tumor photoablation when mixed with cationic liposomes.

As featured in:

See Honglin Jin, Jonathan F. Lovell *et al.*, *Biomater. Sci.*, 2019, **7**, 3158.

ROYAL SOCIETY OF CHEMISTRY | Celebrating IYPT 2019

rsc.li/biomaterials-science

Registered charity number: 207890

Biomaterials Science

PAPER

View Article Online
View Journal | View Issue

Cite this: *Biomater. Sci.*, 2019, **7**, 3158

Indocyanine green binds to DOTAP liposomes for enhanced optical properties and tumor photoablation†

Dyego Miranda,‡[a] Chao Wan,‡[b] Hailey I. Kilian,[a] Moustafa T. Mabrouk,[a] Yuhan Zhou,[b] Honglin Jin *[b] and Jonathan F. Lovell *[a]

Received 7th April 2019,
Accepted 13th June 2019

DOI: 10.1039/c9bm00551j

rsc.li/biomaterials-science

Indocyanine green (ICG) is a clinically-approved near infrared (NIR) dye used for optical imaging. The dye is only slightly soluble in water and is prone to aggregation in saline solutions, so that alternative formulations can improve photophysical performance. Numerous nanoscale formulations of ICG have been described in the literature, but we sought to develop an approach that does not require additional purification steps. Pre-formed liposomes incorporating 45 mol% of the cationic lipid 1,2-dioleoyl-3-trimethylammonium-propane (DOTAP) rapidly bind ICG, resulting in enhanced NIR optical properties. ICG binding is dependent on the amount of DOTAP incorporated in the liposomes. A dye-to-lipid mass ratio of [0.5 : 25] is sufficient for full complexation, without additional purification steps following mixing. NIR absorption, fluorescence intensity, and photoacoustic signals are increased for the liposome-bound dye. Not only is the optical character enhanced by simple mixing of ICG with liposomes, but retention in 4T1 mammary tumors is observed following intratumor injection, as assessed by fluorescence and photoacoustic imaging. Subsequent photothermal therapy with 808 nm laser irradiation is effective and results in tumor ablation without regrowth for at least 30 days. Thus, ICG optical properties and photothermal ablation outcomes can be improved by mixing the dye with pre-formed DOTAP liposomes in conditions that result in full dye-binding to the liposomes.

Introduction

Indocyanine green (ICG) is an FDA-approved near infrared (NIR) dye that has been applied clinically for optical imaging in surgery and oncology.[1,2] The long absorption wavelength (~800 nm) allows for optical imaging in the NIR window, in which light can penetrate deeper into tissues. ICG has aqueous solubility in the low mg mL^{-1} range, which is how the dye is administered clinically. This solubility range is considered to be only slightly soluble. In saline solutions, ICG is especially prone to aggregation, resulting in suboptimal spectral properties.

Given the clinical relevance of ICG, a wide variety of approaches have been developed to formulate the dye with enhanced properties.[3] Liposomes have been used in numerous cases to formulate ICG and other cyanine dyes for optical imaging and phototherapy.[4–10] In some cases, drugs have been combined with ICG liposomes for monitoring drug delivery.[11,12] ICG has also been used to trigger cargo release from liposomes.[13,14] Many other formulations of ICG have been developed including, for example, those based on metallic nanoparticles,[15] silica nanoparticles,[16,17] polymer nanoparticles,[18,19] iron oxide nanoparticles,[20] nanotubes,[21] albumin,[22] and even virus-like particles.[23] Such formulations have advantageous properties as theranostic nanomaterials which integrate optical imaging and therapy.[24,25]

1,2-Dioleoyl-3-trimethylammonium-propane (DOTAP) is a synthetic unsaturated cationic lipid which has been incorporated in liposomes in the EndoTAG taxane formulation undergoing clinical trials.[26] Cationic DOTAP liposomes have altered properties compared to neutral ones, and generally have short circulation and rapidly bind blood vessels following intravenous administration.[27] Notably, DOTAP liposomes have previously been used to encapsulate ICG for assessing lymphatic tracking and biodistribution in immunization studies[28] as well as imaging choroidal angiogenesis.[29]

Contrast-enhanced photothermal therapy (PTT) has been demonstrated for a wide range of materials, beyond those that

[a]*Department of Biomedical Engineering, University at Buffalo, State University of New York, Buffalo, NY 14260, USA*
[b]*Cancer Center, Union Hospital, Tongji Medical College, Huazhong University of Science and Technology, Wuhan 430022, China. E-mail: jflovell@buffalo.edu, jin@hust.edu.cn*

†Electronic supplementary information (ESI) available: ICG spectra and cellular uptake. See DOI: 10.1039/c9bm00551j

‡Equal contribution.

incorporate ICG. These include inorganic material such as gold nanoparticles,[30] carbon nanotubes,[31] graphene,[32] and many others.[33] Organic nanomaterials have also been explored extensively for PTT.[34–36] PTT is an ablative technique that uses NIR lasers to heat and destroy tumors which have accumulated NIR contrast agents. Intratumoral injection of theranostic probes has potential to be used for precise tumor targeting without high systemic toxicity. An optimized liposomal ICG formulation has been shown to be effective for PTT following intratumor injection.[37] This approach was extended to incorporate a chemotherapy agent along with the ICG,[38] for chemophototherapy.[39] ICG has also been loaded into therapeutic hydrogels for intratumoral injection.[40] Liposomes with imaging contrast agents loaded can be used to guide intratumoral injections and plan phototherapy.[41]

In typical ICG nanoscale formulations, ICG is incorporated early in the procedure and then free ICG is removed by techniques such as dialysis or gel filtration, leaving only the entrapped or bound dye. However, such purification adds some additional complexity to the formulation process. In theory, use of a mixing approach which results in full ICG complexation without additional purification could be a simpler approach. In this study, we show that pre-formed DOTAP liposomes can be mixed with an ICG solution to achieve full dye binding, improved optical properties and enhanced PTT.

Results and discussion

ICG binds to liposomes that contain DOTAP

A stock solution of ICG was formed at 1 mg mL^{-1} in phosphate buffered saline (PBS). When ICG was subsequently diluted in a 1 : 1 volume ratio with a DOTAP liposome formulation, enhanced NIR absorption was observed compared to the same dilution in PBS (Fig. 1A). The cationic liposomes incorporated 45 mol% DOTAP, 50 mol% cholesterol and 5 mol% polyethyleneglycol 2000 distearoyl phosphatidylethanolamine (PEG-DSPE). The nature of the absorption increase is likely due to enhanced solubility of the ICG in the lipophilic environment compared to saline solution, as ICG absorption is known to be enhanced with lipids.[42] As shown in Fig. 1B, NIR photoacoustic intensity was greater for ICG when mixed with DOTAP liposomes. This was expected, due to the greater NIR absorption in the colloidal solution, which is responsible for conversion of light into sound. Likewise, Fig. 1C, shows that the florescence

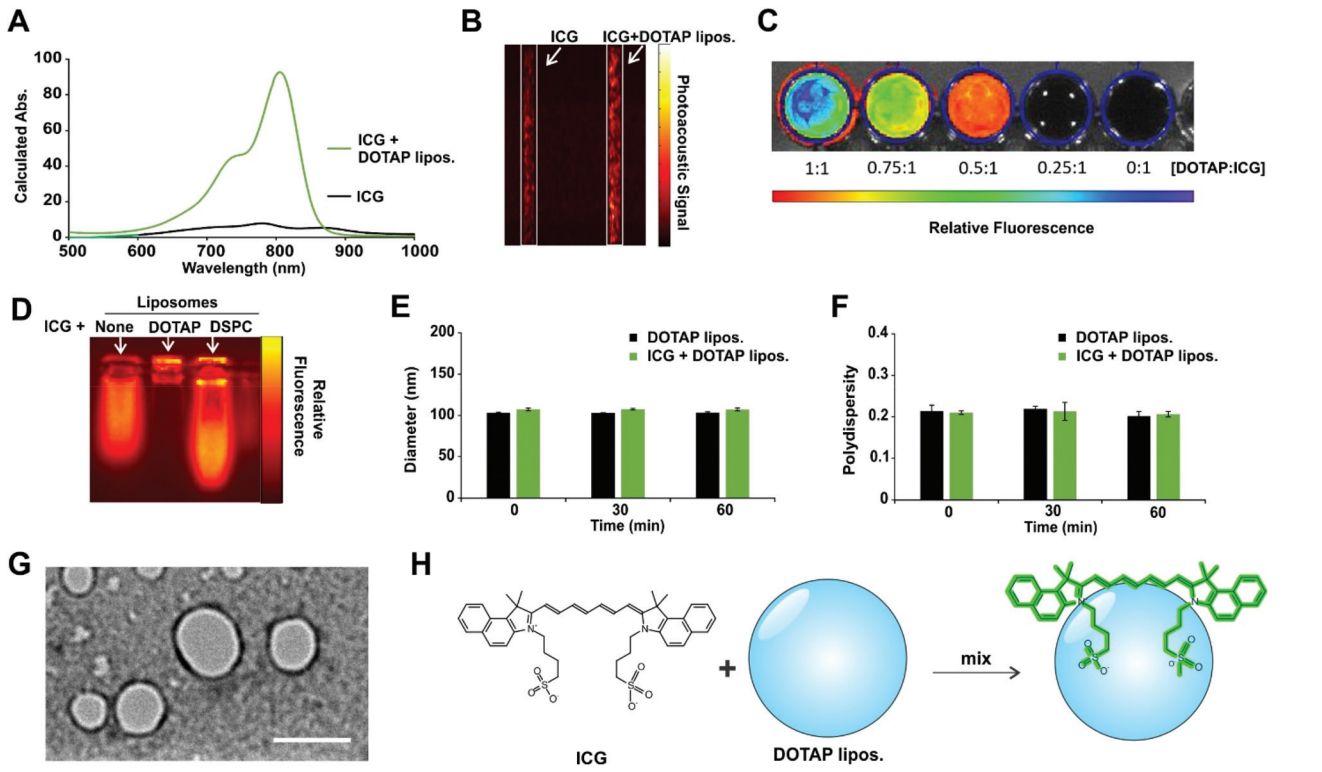

Fig. 1 ICG binds to DOTAP liposomes for enhanced optical properties: (A) calculated absorption (absorption multiplied by the dilution factor, which was 100) of 0.5 mg mL^{-1} ICG in saline, with or without DOTAP liposomes (25 mg mL^{-1} total lipid). (B) Photoacoustic signal of ICG with or without mixing with DOTAP liposomes. (C) Fluorescence of ICG with increasing amounts of DOTAP liposomes. The volume ratios are shown for mixing 1 mg mL^{-1} ICG with 50 mg mL^{-1} liposomes. (D) Agarose gel electrophoresis of ICG, or ICG mixed with DOTAP liposomes or DSPC liposomes. Liposomes size (E) and polydispersity (F) upon incubation with ICG for indicated times. (G) Negative stained transmission electron microscopy of DOTAP liposomes complexed with ICG. A 100 nm scale bar is shown. (H) Schematic representation of the enhancement of ICG photophysical properties (shown by green color) upon mixing and binding to DOTAP liposomes.

increases when ICG is mixed with DOTAP liposomes. In the saline solution, the ICG likely is partially aggregated with quenched fluorescence so minimal fluorescent emission signal is apparent. Mixing ICG with DOTAP liposomes results in better dye solubilization, leading to higher fluorescence.

To confirm the nature of the enhanced optical properties was due to dye binding to the liposomes, an electrophoresis gel shift assay was carried out (Fig. 1D). ICG was mixed with liposomes for a final concentration of 0.5 mg mL^{-1} ICG and 25 mg mL^{-1} liposomes. Free ICG is negatively charged and therefore moved towards the cathode. In contrast, cationic DOTAP liposomes completely bound all the free ICG at that liposome and dye ratio. As a result, no free dye migrated. The third well was loaded with ICG that was mixed with neutral liposomes formed from the saturated lipid distearoylphosphatidylcholine (DSPC). In this case, ICG migrated towards the cathode than similarly to the free dye. Since liposomes migrate slowly in the gel, the lack of dye near the loading well indicates minimal dye bound the DSPC liposomes. The electrophoresis result provides direct proof of ICG binding to DOTAP liposomes. Mixing ICG with DSPC liposomes also did not provide for as strong absorption as DOTAP liposomes (Fig. S1 in the ESI†). Interestingly, liposomes formed from DOTAP or another unsaturated lipid, dipalmitoylphosphatidylcholine (DOPC), both provided for similarly strong ICG absorption, suggesting that ICG interaction with liposomes may be enhanced by the presence unsaturated lipids. This is in agreement with a prior study that found that compared to DSPC, a DOPC-based formulation, also containing 5 mol% PEG, was optimal for fluorescence imaging and PTT.[37]

The size of DOTAP liposomes was assessed 30 and 60 minutes following mixing with ICG to induce dye binding (Fig. 1E). No major changes in particle size were induced by ICG binding. Liposome sizes remained close to 100 nm. Likewise, the liposomes did not increase in polydispersity upon ICG binding (Fig. 1F). The morphology of the liposomes remained intact after ICG binding (Fig. 1G). These data show that ICG binding to DOTAP liposomes does not induce liposome aggregation. A simple schematic is presented in Fig. 1H, in which ICG is mixed with DOTAP liposomes, resulting in enhanced optical properties upon dye binding.

Given that ICG bound to unsaturated DOTAP liposomes, relative to saturated DSPC liposomes, we assessed ICG binding as a function of the amount of DOTAP present. Cholesterol and DSPE-PEG were kept constant at 50% to 5%, respectively, while DOTAP was titrated in place of DSPC. As shown in Fig. 2A, as DOTAP content was increased, ICG binding increased, and full ICG binding was observed with 45 mol% DOTAP. Next, using 45 mol% DOTAP liposomes, the amount of liposomes was varied to examine the relation with ICG binding (Fig. 2B). Full binding of 0.5 mg mL^{-1} ICG was observed with 25 mg mL^{-1} lipid. Since the lipid formulation also comprised DSPE-PEG, we assessed whether PEG was essential for ICG binding. As shown in Fig. 2C, full

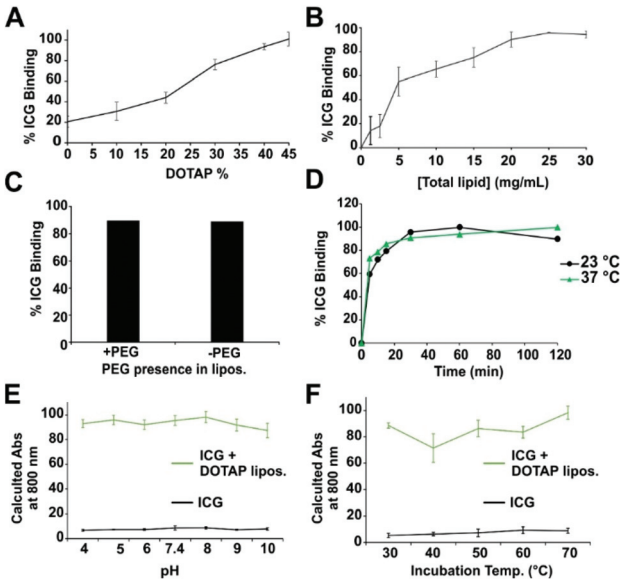

Fig. 2 Characterizing ICG binding to DOTAP liposomes: (A) ICG binding to liposomes containing variable amounts of DOTAP. (B) ICG binding to DOTAP liposomes (45 mol% DOTAP) with varying liposome concentration. (C) Binding of ICG to DOTAP liposomes with or without 5 mol% PEG-DSPE included. (D) Kinetics of ICG binding to DOTAP liposomes at indicated temperatures. Calculated absorption values of ICG at 800 nm with or without DOTAP liposomes following incubation at varying pH (E) or elevated temperatures (F). Error bars reflect mean ± std. dev. for $n = 3$ samples.

binding was achieved with or without DOTAP liposome PEGylation.

The binding kinetics between ICG and DOTAP liposomes was compared at 23 and 37 °C (Fig. 2D). No major differences in binding were observed at these temperatures. Most of the binding was complete in less than 30 minutes. The stability of ICG complexed with DOTAP liposomes was inspected in varying pH and temperature conditions. Based on the increased absorbance at 800 nm compared to the free dye, ICG remained stably bound to DOTAP liposomes in a wide pH range (Fig. 2E). Likewise, after ICG or liposome-bound ICG was incubated for 30 minutes at elevated temperatures, no decrease in NIR absorption was observed, showing thermostable binding of the dye to the liposomes.

Optical imaging following intratumoral injection

To visualize the tumor uptake of free ICG compared to ICG mixed with DOTAP liposomes, mice bearing 4T1 orthotopic mammary tumors were used. When the average volume reached approximately 75 mm^3, tumors were directly injected with ICG with or without DOTAP liposomes. 24 hours after intratumoral injection, the dye that had been mixed with DOTAP liposomes prior to injection showed superior retention and distribution in the tumors, compared to the free dye (Fig. 3A). Several of the 5 mice injected with the free dye had no signal remaining in the tumor 24 hours following injection and the other mice in that group had relatively weak signal. In

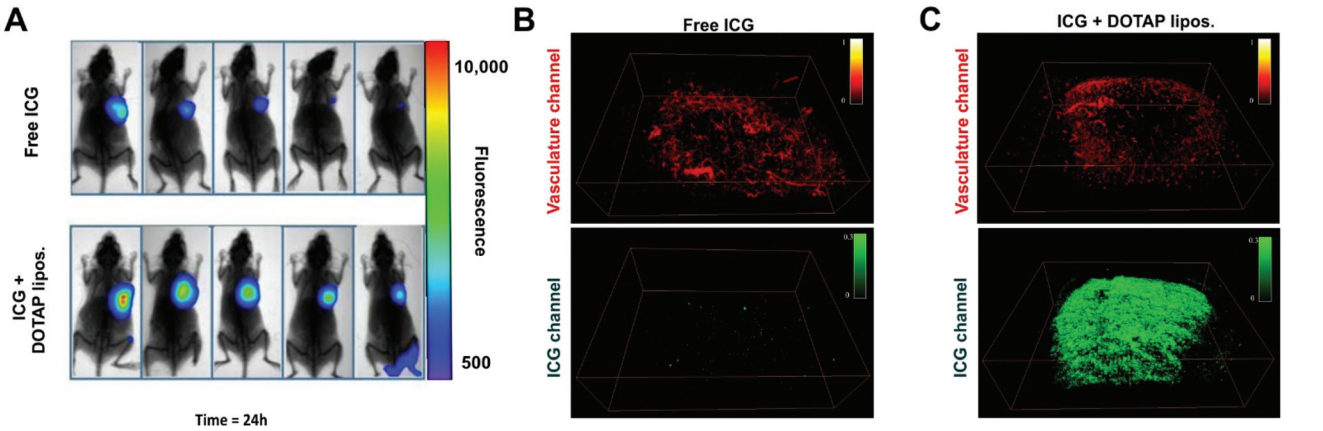

Fig. 3 NIR fluorescence and photoacoustic tumor imaging of ICG with or without mixing with DOTAP liposomes. (A) Fluorescence imaging of 4T1-bearing mice 24 hours after intratumoral injection of ICG with or without complexing with DOTAP liposomes. Representative photoacoustic image of free ICG (B) or ICG complexed with DOTAP liposomes (C), 24 hours after intratumoral injection. The top image in red shows the tumor blood vessels and the bottom image in green shows ICG distribution in the tumor.

contrast, all the mice injected with ICG complexed with DOTAP retained a strong fluorescence signal in the tumor. Further research is required to better elucidate the mechanism of enhanced tumor retention of the DOTAP formulation, but it is likely that the larger size of the liposomal ICG may have retarded drainage of the small molecule ICG from the tumor. Furthermore, the cationic character of the liposomes may have led to more interaction with various cell membranes in the tumor, which carry a mild anionic charge. Incubation of ICG with 4T1 cells *in vitro* revealed that, compared to the free dye, ICG mixed with DOTAP liposomes was uptaken more avidly (Fig. S2 in the ESI†).

Fig. 3B shows a representative photoacoustic tomography image of a tumor 24 hours after injection with free ICG. The blood vessels of the tumor are shown in red (top image) and are based on endogenous absorption from hemoglobin. The ICG signal is shown in green (bottom image). Minimal ICG signal is present in the free ICG-injected mice. Fig. 3C shows a representative photoacoustic image of a tumor injected with ICG complexed with DOTAP liposomes. Whereas the tumor blood vasculature appears comparable to the free ICG injection, the photoacoustic contrast image reveals greatly stronger ICG signal. The photoacoustic image reveals that the ICG is relatively well-distributed throughout the tumor volume.

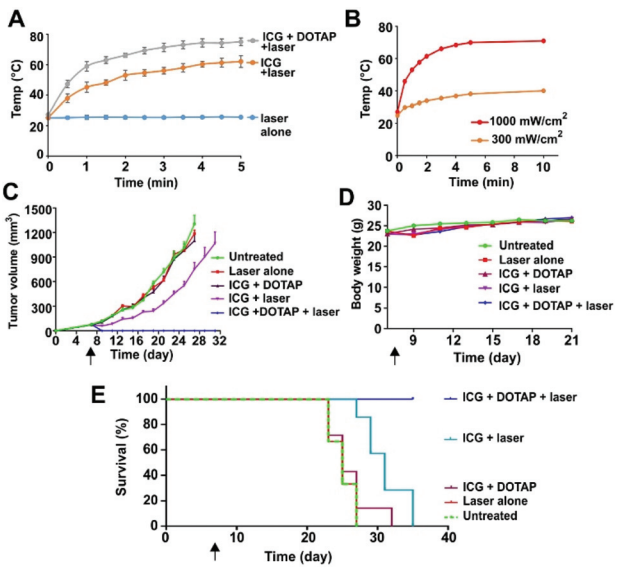

Fig. 4 Photothermal therapy with ICG and DOTAP liposomes. (A) Temperature of ICG solutions under 808 nm laser irradiation. (B) Temperature of ICG mixed with DOTAP liposomes at two different laser fluence rates. (C) Mice were inoculated with orthotopic 4T1 tumors on day 0, then on day 7 were injected intratumorally with ICG (25 μg). 24 hours later, tumors were treated with an 808 nm laser (0.75 W cm^{-2}, 8 min). n = 6–7 mice per group. (D) The body weight of mice over the course of treatment (E) survival for indicated groups. Arrow shows the time of the single PTT treatment.

Photothermal therapy

Under 808 nm irradiation, ICG with and without mixing with DOTAP liposomes resulted in production of photothermal heating (Fig. 4A). Owing to the higher NIR absorption, liposome-bound ICG was more effective at photothermal transduction. Tumor cells are thermally damaged at temperatures above 40 °C and coagulative necrosis and ablation occurs at temperatures above 60 °C with rapid denaturing of proteins and cellular membrane collapse. As seen in Fig. 4B, ICG mixed with DOTAP liposomes exposed to 1000 mW cm^{-2} laser power the temperature plateaued at ~70 °C after a few minutes of irradiation, whereas a lower fluence rate produced less heating.

Tumors were injected with ICG and subjected to laser irradiation 24 hours later. Several reports have suggested that photodynamic therapy, along with PTT, contributes to ICG mechanism of action, which is possible in this case.[9,43–45] As shown in Fig. 4C, the tumor volumes of three controls had little difference between them: (1) untreated; (2) laser alone;

and (3) ICG mixed with DOTAP liposomes without laser. The tumor volumes of these groups increased steadily over the study period. The ICG with laser treatment group had a slight impact on tumor growth, as this treatment likely resulted in some minor heating. In contrast to the other groups, ICG with DOTAP liposomes and laser treatment resulted in tumor ablation with a single laser treatment due to the increased photothermal properties of complexed ICG as well as improved dye retention in the tumor. ICG and DOTAP liposome treatment had low systemic toxicity, as seen in Fig. 4D, as the mice were able to increase or maintain their body weight. However, additional toxicity studies are warranted. Due to the enhanced photothermal effect, mice phototreated with ICG and DOTAP liposomes displayed 100% survival at 40 days post tumor inoculation (Fig. 4E).

Conclusion

In this work, we demonstrated that simple mixing of ICG with DOTAP liposomes can result in full dye binding to the liposomes and enhanced ICG optical properties. Greater NIR fluorescence and photoacoustic signal generation can be used for improved contrast imaging. Tumor retention also appeared superior following intratumoral injection of ICG complexed with DOTAP liposomes. These factors resulted in effective photothermal ablation of orthotopic mammary tumors in mice. Taken together, these results demonstrate a simple route to improving the efficacy of ICG by simply mixing the dye with pre-formed liposomes.

Experimental

Materials

Indocyanine green (ICG) was obtained from Chem-Impex International Inc. Lipids were purchased from CordenPharma and included 2,3-dioleoyloxy-propyl-trimethyammoniumchloride (DOTAP, # LP-R4-117), 1,2-distearoyl-*sn-glycero*-3-phosphocholine (DSPC, # LP-R4-076), 1,2-distearoyl-*sn-glycero*-3-phosphoethanolamine-*N*-(methoxy(PEG)-2000 (MPEG-2000-DSPE, # LP-R4-039), and 1,2-dioleoyl-*sn-glycero*-3-phosphocholine (DOPC, # LP-R4-070). Cholesterol was purchased from Nu-Chek Prep, Inc. (#CH-800-A28-Z). Other chemicals were from Sigma. The 4T1 cell line (BALB/c mouse breast carcinoma) was kindly provided by Bo Huang (Peking Union Medical College, Beijing, China). Six- to eight-week-old female BALB/c mice were obtained from HBCDC (Wuhan, China).

Liposomes

Lipids were dissolved in chloroform and dispensed in a glass test tube and the chloroform was evaporated by nitrogen gas flow. The molar ratio of Chol : DOTAP : DSPE-PEG was 10 : 9 : 1. 1 mL of PBS (150 mM NaCl, 10 mM phosphate buffer) at 60 °C was added and the lipids were sonicated for 30 min in a water bath at 60 °C. DSPC and DOPC liposomes were formed in the same way, by substituting those lipids for DOTAP. The size and polydispersity of DOTAP liposomes was determined by dynamic light scattering in a NanoBrook 90 plus PALS instrument. Electron microscopy was carried out with a JEM-2010 electron microscope with liposomes that were placed on a grid and negative stained with uranyl acetate.

ICG binding to liposomes

A 1 mg mL^{-1} ICG solution was mixed with liposomes, to generate a final concentration of 0.5 mg mL^{-1} ICG and 25 mg mL^{-1} total lipid. This mixture was incubated for 1 h at 37 °C with shaking. Samples were diluted 100 fold and absorbance was measured with a PerkinElmer Lambda 365 UV-Vis Spectrophotometer. Binding could be quantified by measuring absorption after passing samples through a 0.2 μm nylon syringe filter (Agilent # 5190-5269), which we found adsorbs free ICG. For gel electrophoresis, a 2% agarose gel was used with Tris, acetic acid and EDTA (TAE) buffer. To visualize the fluorescence of ICG the samples were imaged using an IVIS Lumina imager. For pH stability the ICG samples were diluted by 100 fold into phosphate buffer of the indicated pH, incubated for 30 min at room temperature prior to measurement. For temperature stability, the samples were incubated for 30 min at the indicated temperatures, then rapidly diluted 100 fold into a PBS and absorbance measurement. For *in vitro* uptake of liposomes 4T1 cells (4×10^5 cells per well) were seeded into a 6-well plate with 2 mL RPMI 1640 medium for 12 h. Then, 5 μL of ICG solution (containing 0.5 mg mL^{-1} ICG) with or without DOTAP liposomes was added. Cells were harvested at 6 or 12 h, washed with PBS, and ICG was detected with flow cytometry.

In vivo imaging

All animal studies were performed in compliance with protocols approved by the Hubei Provincial Animal Care and Use Committee, following the experimental guidelines of the Animal Experimentation Ethics Committee of the Huazhong University of Science and Technology (HUST, Wuhan, China). 5×10^5 4T1 cells in 50 μL PBS were inoculated into the right second breast pad of female BALB/c mice. When the average tumor volume reached approximately 75 mm^3, mice were allocated into two groups randomly. Mice in the ICG group were intratumorally injected with 50 μL of free ICG solution (containing 0.25 mg mL^{-1} ICG), and mice in the ICG-LIP group were intratumorally injected with 50 μL of ICG-LIP (containing 0.25 mg mL^{-1} ICG). For the semiquantitative fluorescence analysis of ICG at 0, 6, and 24 h after injection, a Spectral Instruments Imaging Optical Imaging Platform equipped with an excitation filter (750 nm) and emission filter (790 nm) was used to collect ICG fluorescence signals. For photoacoustic imaging, 4T1 murine tumor-bearing female BALB/c mice were intratumorally injected with free ICG solution (50 μL of 0.5 mg mL^{-1} ICG) or ICG with DOTAP liposomes (50 μL of 0.5 mg mL^{-1} ICG). PAT imaging was carried out 24 h after injection. Mice were scanned using a multispectral optoacoustic tomography (MSOT inVision 128, iThera Medical GmbH,

Germany). Photoacoustic signals of blood vessels and ICG were recorded at excitation wavelengths of 532 and 710 nm, respectively.

Photothermal therapy

In vitro photothermal measurements were carried out with a 1 mL sample volume in microcentrifuge tubes which were exposed to 808 nm laser irradiation. Temperatures were recorded with an infrared FLIR thermal camera. For *in vivo* studies, female BALB/c mice were inoculated in the mammary fat pad with 4T1 cells and on day 7, when tumor volumes reached approximately 75 mm^3, mice were allocated randomly into the following five groups (6–7 mice in each group): (a) untreated, (b) laser alone, (c) ICG solution with laser treatment (50 μL, containing 0.5 mg mL^{-1} ICG), (d) ICG with DOTAP liposomes alone (50 μL, containing 0.5 mg mL^{-1} ICG) and (e) ICG with DOTAP liposomes (50 μL, containing 0.5 mg mL^{-1} ICG) with laser treatment. The samples were intratumorally injected. 24 h after injection, the tumors of groups (b), (c) and (e) were irradiated with an 808 nm laser (0.75 W cm^{-2}, 8 min). The tumor size was measured using a caliper every other day. The mice were sacrificed after tumor volume exceeded 1000 mm^3.

Conflicts of interest

The authors declare no competing interests.

Acknowledgements

This work was supported by the National Institutes of Health (R01EB017270 and DP5OD017898), the National Science Foundation (1555220), a Brazilian CAPES Science without Borders scholarship (D. M.) and a Fulbright Scholarship (M. T. M.).

References

1 K. Polom, D. Murawa, Y.-S. Rho, P. Nowaczyk, M. Hünerbein and P. Murawa, *Cancer*, 2011, **117**, 4812–4822.
2 M. V. Marshall, J. C. Rasmussen, I. C. Tan, M. B. Aldrich, K. E. Adams, X. Wang, C. E. Fife, E. A. Maus, L. A. Smith and E. M. Sevick-Muraca, *Open Surg. Oncol. J.*, 2010, **2**, 12–25.
3 Z. Sheng, D. Hu, M. Xue, M. He, P. Gong and L. Cai, *Nano-Micro Lett.*, 2013, **5**, 145–150.
4 N. Beziere, N. Lozano, A. Nunes, J. Salichs, D. Queiros, K. Kostarelos and V. Ntziachristos, *Biomaterials*, 2015, **37**, 415–424.
5 X. Zhang, N. Li, Y. Liu, B. Ji, Q. Wang, M. Wang, K. Dai and D. Gao, *Nanomedicine*, 2016, **12**, 2019–2029.
6 H. S. Jeong, C. M. Lee, S. J. Cheong, E. M. Kim, H. Hwang, K. S. Na, S. T. Lim, M. H. Sohn and H. J. Jeong, *J. Liposome Res.*, 2013, **23**, 291–297.
7 S. T. Proulx, P. Luciani, S. Derzsi, M. Rinderknecht, V. Mumprecht, J. C. Leroux and M. Detmar, *Cancer Res.*, 2010, **70**, 7053–7062.
8 M. Mikada, A. Sukhbaatar, Y. Miura, S. Horie, M. Sakamoto, S. Mori and T. Kodama, *Cancer Sci.*, 2017, **108**, 846–852.
9 F. Yan, H. Wu, H. Liu, Z. Deng, H. Liu, W. Duan, X. Liu and H. Zheng, *J. Controlled Release*, 2016, **224**, 217–228.
10 D. Miranda, H. Huang, H. Kang, Y. Zhan, D. Wang, Y. Zhou, J. Geng, H. I. Kilian, W. Stiles, A. Razi, J. Ortega, J. Xia, H. S. Choi and J. F. Lovell, *Theranostics*, 2019, **9**, 381–390.
11 N. Lozano, Z. S. Al-Ahmady, N. S. Beziere, V. Ntziachristos and K. Kostarelos, *Int. J. Pharm.*, 2015, **482**, 2–10.
12 X. Xue, T. Fang, L. Yin, J. Jiang, Y. He, Y. Dai and D. Wang, *Drug Delivery*, 2018, **25**, 1826–1839.
13 T. Lajunen, R. Nurmi, D. Wilbie, T. Ruoslahti, N. G. Johansson, O. Korhonen, T. Rog, A. Bunker, M. Ruponen and A. Urtti, *J. Controlled Release*, 2018, **284**, 213–223.
14 T. Lajunen, L.-S. Kontturi, L. Viitala, M. Manna, O. Cramariuc, T. Róg, A. Bunker, T. Laaksonen, T. Viitala, L. Murtomäki and A. Urtti, *Mol. Pharm.*, 2016, **13**, 2095–2107.
15 L. Han, Y. Zhang, X.-W. Chen, Y. Shu and J.-H. Wang, *J. Mater. Chem. B*, 2016, **4**, 105–112.
16 G. Ferrauto, F. Carniato, E. Di Gregorio, L. Tei, M. Botta and S. Aime, *Nanoscale*, 2017, **9**, 99–103.
17 P. Sharma, N. E. Bengtsson, G. A. Walter, H.-B. Sohn, G. Zhou, N. Iwakuma, H. Zeng, S. R. Grobmyer, E. W. Scott and B. M. Moudgil, *Small*, 2012, **8**, 2856–2868.
18 M. Zheng, C. Yue, Y. Ma, P. Gong, P. Zhao, C. Zheng, Z. Sheng, P. Zhang, Z. Wang and L. Cai, *ACS Nano*, 2013, **7**, 2056–2067.
19 V. Saxena, M. Sadoqi and J. Shao, *J. Photochem. Photobiol., B*, 2004, **74**, 29–38.
20 Y. Ma, S. Tong, G. Bao, C. Gao and Z. Dai, *Biomaterials*, 2013, **34**, 7706–7714.
21 G. Wang, F. Zhang, R. Tian, L. Zhang, G. Fu, L. Yang and L. Zhu, *ACS Appl. Mater. Interfaces*, 2016, **8**, 5608–5617.
22 Z. Sheng, D. Hu, M. Zheng, P. Zhao, H. Liu, D. Gao, P. Gong, G. Gao, P. Zhang, Y. Ma and L. Cai, *ACS Nano*, 2014, **8**, 12310–12322.
23 W. Shan, R. Chen, Q. Zhang, J. Zhao, B. Chen, X. Zhou, S. Ye, S. Bi, L. Nie and L. Ren, *Adv. Mater.*, 2018, **30**, 1707567.
24 L. Cheng, C. Wang, L. Feng, K. Yang and Z. Liu, *Chem. Rev.*, 2014, **114**, 10869–10939.
25 H. Huang and J. F. Lovell, *Adv. Funct. Mater.*, 2017, **27**, 1603524.
26 U. Fasol, A. Frost, M. Büchert, J. Arends, U. Fiedler, D. Scharr, J. Scheuenpflug and K. Mross, *Ann. Oncol.*, 2012, **23**, 1030–1036.
27 D. Luo, J. Geng, N. Li, K. A. Carter, S. Shao, G. E. Atilla-Gokcumen and J. F. Lovell, *Mol. Cancer Ther.*, 2017, **16**, 2452–2461.

28 Y. Zhuang, Y. Ma, C. Wang, L. Hai, C. Yan, Y. Zhang, F. Liu and L. Cai, *J. Controlled Release*, 2012, **159**, 135–142.
29 J. Hua, N. Gross, B. Schulze, U. Michaelis, H. Bohnenkamp, E. Guenzi, L. L. Hansen, G. Martin and H. T. Agostini, *Mol. Vision*, 2012, **18**, 1045–1054.
30 X. Huang and M. A. El-Sayed, *J. Adv. Res.*, 2010, **1**, 13–28.
31 N. W. S. Kam, M. O'Connell, J. A. Wisdom and H. Dai, *Proc. Natl. Acad. Sci. U. S. A.*, 2005, **102**, 11600–11605.
32 K. Yang, S. Zhang, G. Zhang, X. Sun, S.-T. Lee and Z. Liu, *Nano Lett.*, 2010, **10**, 3318–3323.
33 Z. Bao, X. Liu, Y. Liu, H. Liu and K. Zhao, *Asian J. Pharm. Sci.*, 2016, **11**, 349–364.
34 J. F. Lovell, C. S. Jin, E. Huynh, H. Jin, C. Kim, J. L. Rubinstein, W. C. W. Chan, W. Cao, L. V. Wang and G. Zheng, *Nat. Mater.*, 2011, **10**, 324–332.
35 Y. Lyu, Y. Fang, Q. Miao, X. Zhen, D. Ding and K. Pu, *ACS Nano*, 2016, **10**, 4472–4481.
36 Y. Zhang, H. Hong, B. Sun, K. Carter, Y. Qin, W. Wei, D. Wang, M. Jeon, J. Geng, R. J. Nickles, G. Chen, P. N. Prasad, C. Kim, J. Xia, W. Cai and J. F. Lovell, *Nanoscale*, 2017, **9**, 3391–3398.
37 H.-J. Yoon, H.-S. Lee, J.-Y. Lim and J.-H. Park, *ACS Appl. Mater. Interfaces*, 2017, **9**, 5683–5691.
38 H.-J. Yoon, H.-S. Lee, J.-H. Jung, H. K. Kim and J.-H. Park, *ACS Appl. Mater. Interfaces*, 2018, **10**, 6118–6123.
39 D. Luo, K. A. Carter, D. Miranda and J. F. Lovell, *Adv. Sci.*, 2017, **4**, 1600106.
40 H. Jin, G. Zhao, J. Hu, Q. Ren, K. Yang, C. Wan, A. Huang, P. Li, J.-P. Feng, J. Chen and Z. Zou, *ACS Appl. Mater. Interfaces*, 2017, **9**, 25755–25766.
41 D. Miranda, K. Carter, D. Luo, S. Shao, J. Geng, C. Li, U. Chitgupi, S. G. Turowski, N. Li, G. E. Atilla-Gokcumen, J. A. Spernyak and J. F. Lovell, *Adv. Healthcare Mater.*, 2017, **6**, 1700253.
42 J. C. Kraft and R. J. Y. Ho, *Biochemistry*, 2014, **53**, 1275–1283.
43 C. Shirata, J. Kaneko, Y. Inagaki, T. Kokudo, M. Sato, S. Kiritani, N. Akamatsu, J. Arita, Y. Sakamoto, K. Hasegawa and N. Kokudo, *Sci. Rep.*, 2017, **7**, 13958.
44 K. Deng, Z. Hou, X. Deng, P. Yang, C. Li and J. Lin, *Adv. Funct. Mater.*, 2015, **25**, 7280–7290.
45 W. Song, Y. Li, Y. Wang, D. Wang, D. He, W. Chen, W. Yin and W. Yang, *J. Biomed. Nanotechnol.*, 2017, **13**, 1115–1123.

